Topological study, using a coupled ELF and catastrophe theory technique, of electron transfer in the Li + Cl_2 system†

Xénophon Krokidis,*[a] Bernard Silvi,[a] Christine Dezarnaud-Dandine[b] and Alain Sevin[a]

[a] *Laboratoire de Chimie Théorique, Université Pierre et Marie Curie, 4 Place Jussieu, 75252 Paris cedex 05, France*
[b] *Laboratoire de Chimie Physique–Matière et Rayonnement, Université Paris 6, 11, Rue Pierre et Marie Curie, 75231 Paris cedex 05, France*

A topological study of electron transfer in the {Li + Cl_2} system, based on catastrophe theory and using ELF as a starting point, has been achieved. It enables the determination of the method-independent invariants that might be used for characterizing the well-documented harpooning process in all types of geometry. This study has shown that the process is characterized by an electron jump from the covalent {Li + Cl_2} state, stable at large separation distances, to the ionic charge transfer state {Li^+ + Cl_2^-}. The topological invariant associated with this behaviour is a dual cusp catastrophe, whose existence has been found at any level of calculation, that is, MP2, DFT and CASSCF. The latter catastrophe is mostly associated with the actual cleavage of the Cl_2^- species. Analysis of the topological parameters allows the actual regions of PES crossings, in any geometry, to be localized. Our results suggest that the dual cusp catastrophe characterizes the diabatic surface crossings that are subjacent in the classical adiabatic analysis of the overall reaction path.

Electron transfer in metal plus dihalogen or related systems has been the subject of much experimental and theoretical work, and is generally considered as taking place through the so-called 'harpooning mechanism'.[1] Our work was aimed at studying this mechanism by considering the modifications occurring in the bonding pattern of the system induced by the electron transfer. A chemical process can be characterized by the changes occurring in bonding as a function of the nuclear configurations. In this perspective, a non-empirical qualitative study of bond making and breaking requires the definition of simple concepts associated with the chemical properties of the system.

Topology provides a firm basis for this analysis and several qualitative frameworks have become classical. The most well known is *conservation of the local symmetry of occupied molecular orbitals* (*MOs*),[2–4] leading to Woodward and Hoffmann's rules.[5] In the same spirit, Salem, Dauben and Turro[6–8] introduced the notion of *topicity*. Lastly, the concept of MO-and-state *natural correlations* has been proposed.[9–12] The latter method is based on a hierarchy of correlation principles based on conservation of (*i*) local symmetry and (*ii*) dominant electronic localization. Obviously, the second criterion is essential in this approach. In more recent terms, it might be considered that, roughly speaking, the first two methods rely on *adiabatic* correlation schemes, in which *only* MOs and states of different symmetries are allowed to cross along a given path.[13] In contrast, the last method takes into account the possibility of *diabatic* state crossings preserving the initial electron localization in MOs and states of interest.[14] In the latter context, the avoided crossings, obtained in the adiabatic calculation step, exist as the *memory* of the intended diabatic correlations. It is noteworthy that the concept of natural correlations bears a strong analogy with the localized valence bond (VB) description of a reaction process. The strict analogy between both approaches has been shown in studies of chemical and physical quenching of excited light atoms by small molecules.[15] Alternatively, the topological theories of bonding, based on an analysis of the gradient field of well-defined local functions, evaluated from any quantum mechanical method, are close to chemists' intuition and experience and provide method-independent techniques.[16–18]

In this work, we have used the concepts developed in bonding evolution theory[19] (BET, see Appendix B), applied to the electron localization function (ELF, see Appendix A).[20] The latter approach focuses on the evolution of chemical properties by assuming an isomorphism between chemical structures and the *molecular graph* defined in Appendix C. We are aware that the latter approach imposes additional difficulties upon the reader unfamiliar with these concepts. For this reason, four Appendices (A–D), presenting and defining in a concise form the mathematical foundations of the topological description of chemical bonding and reactions, have been added at the end of the article.

The aim of the present study was threefold: (*i*) to describe precisely the nature of the topological invariants associated with the harpooning electron capture; (*ii*) to establish that the topology is largely independent of the quantum mechanical method, provided the latter is of adequate quality; and (*iii*) to show that the small set of control parameters determined by catastrophe theory with a small number of model calculations might be used for the study of any geometry. Our study has been performed in two steps; first, quantum mechanical calculations have been carried out in order to get density matrices. In the second step, these outputs have been used as the starting material for the topological study.

Methodolgy

The quantum mechanical calculations have been performed with the Gaussian 94[21] and the HONDO95-6[22] series of programs. Various levels of electronic correlation have been used throughout: MP2, DFT/B3LYP, CASSCF/MP2[23] and CASSCF/Average,[24,25] with the 6-31G* and 6-311G(3df) basis set.[26] For the sake of brevity, yet illustrating the generality and versatility of our topological approach, we have

† Non-SI units employed: 1 eV ≈ 9.65 J mol^{-1}; 1 a.u. ≈ 2.63 × 10^6 J mol^{-1}.

restricted ourselves to selected results in the upcoming sections: MP2/6-311G(3df) and DFT/B3LYP/6-311G(3df) calculations for the study of C_{2v} and $C_{\infty v}$ geometries; CASSCF/MP2/6-31G* and CASSCF/Average/6-31G* calculations (two lowest energy roots) in the C_s geometry. All CASSCF runs were built according to a (1,5) scheme, using 5 reference configurations of the odd electron. It is noteworthy that, although both CASSCF methods yield similar results far from the conical intersection that characterizes the electronic process, only the CASSCF/Average method gives reliable results in this critical region. The latter calculation requires several runs for each root and, accordingly, the 6-31G* basis set was used so as to obtain a noticeable gain of computing time.

Some selected results, including the isolated partners as well as the complexes, in various geometries are given in Table 1. For example, the calculated vertical electron affinity (EA) of Cl_2 is 0.55 eV at the MP2/6-311G(3df) and 0.9 eV at the B3LYP/6-311G(3df) levels. It is noteworthy that both methods yield very comparable geometrical parameters and relative energies, as can be seen in Table 1. In all calculations involving doublet species, we have checked that spin contamination remained very small and was not likely to affect significantly the corresponding calculated energies. The calculated geometries and energies of the stationary points are given in Table 1. It is worth recalling that these calculations were not aimed at describing the energetics of the Li + Cl_2 system as accurately as possible, but at providing reliable data for further topological exploitation using the BET method.

The topological analysis has been performed with the TopMoD series of programs written in our laboratory.[27] These programs use as input the *wfn* file generated by GAUSSIAN94, with natural orbital populations. The calculations are then carried out in four steps: (*i*) evaluation of the ELF function over a 3D grid; (*ii*) localization of the critical points of the ELF function; (*iii*) identification of the various basins and assignment of the corresponding grid points; (*iv*) integration of charge density over the basins.

Quantum Mechanical Study

To reproduce as closely as possible diabatic conditions, we have fixed the Cl—Cl bond length at its neutral equilibrium value. In this way, the system depends on two parameters as shown in Fig. 1. Previous experimental and theoretical studies on similar systems[1,13,28] have shown that an electron jump from Li to the acceptor molecule Cl_2, which has a positive vertical electron affinity (see Table 1), is likely to take place at a distance *d* (see the definition of this parameter in Fig. 1),

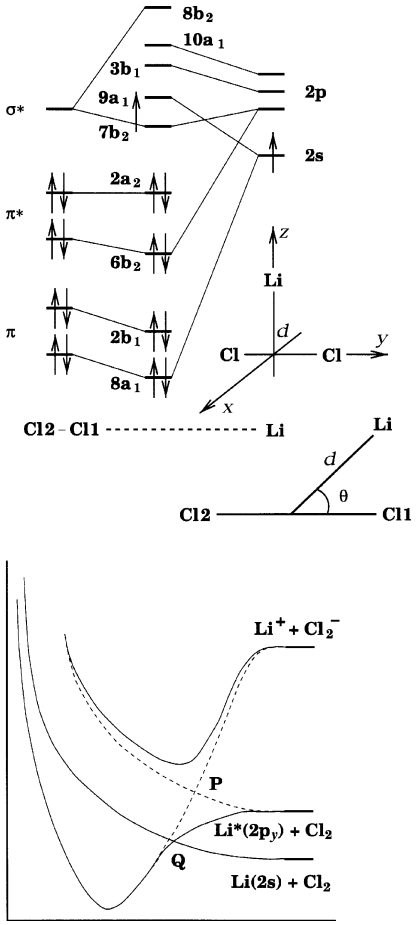

Fig. 1 Qualitative MO-and-states correlation diagram for Li + Cl_2 in the C_{2v} geometry

which is superior to the LiCl equilibrium distance (MP2 value, 2.0425 Å and DFT value, 2.0221 Å). The description of this phenomenon in terms of MOs and states will be briefly recalled in the next section.

MO interactions in the C_{2v} geometry

A schematic interaction diagram for Cl_2 (left) and Li (right) in an isoceles (C_{2v}) geometry is displayed in the upper part of Fig. 1. The ordering and labelling of the electronic levels of the resulting system are those of the calculated MOs. The frontier MOs of Cl_2 have been restricted to the degenerate π and π* sets, respectively composed of in-phase and out-of-phase com-

Table 1 Experimental and calculated structures and energies of the stationary points

		MP2		DFT		Expt.[38]
Species	*d*/Å, θ/°	*E*/a.u.	Δ*E*/eV	*E*/a.u.	Δ*E*/eV	Δ*E*/eV
Li		−7.432	0.00	−7.491	0.00	1.84
Li(^2P)			1.84			1.84
Li^+			5.02		5.62	5.4
Cl		−459.632	0.00	−460.167	0.00	
Cl^-			−3.55		−3.62	−3.62
	MP2, DFT					
Cl_2 (equil.)	1.9854, 2.0112	−919.355	0.00	−920.422	0.00	
Cl_2^- (vertical)		−919.375	−0.55	−920.458	−0.98	
Cl_2^-	2.596, 2.2723	−919.443	−2.40	−920.527	−2.86	2.4–2.5
Li + Cl_2[a]	∞	−926.787	0.00	−927.913	0.00	
	1.94,[b] 90.0	−926.842	−1.50	−927.978	−1.69	
	2.68,[b] 45.0	−926.826	−1.07	−927.963	−1.35	
	3.21,[b] 0.0	−926.821	−0.92	−927.958	−1.20	

[a] Cl_2 non-relaxed for all 4 entries. [b] $d = d_e$ are the MP2 equilibrium values; DFT and CASSCF values are given in the text.

binations of 3p AOs (atomic orbitals) of both Cl atoms, representing the 4 lone pairs of π symmetry. At slightly higher energy one finds the lowest antibonding level, which is the valence σ^* MO. For the Li atom we have reported the valence 2s and 2p sets of AOs. Two types of interactions are worth considering. (*i*) The $8a_1$ MO of Cl_2 interacts in a repulsive fashion with the 2s of Li, yielding the destabilized $9a_1$ MO of the system. This repulsion sharply increases at short distance. (*ii*) The $7b_2$ MO results from the interaction of $6b_2$ and σ^* on Cl_2, on the one hand, and $2p_y$ of Li on the other hand. At short distances, the σ^*–$2p_y$ stabilizing interaction dominates over the $6b_2$–$2p_y$ destabilization, and $7b_2$ might be significantly stabilized. Thus, we see that at short interaction distances, two different MOs compete for the odd electron. When $9a_1$ is populated, the electron is mainly located on Li, yielding a covalent $^2A_1$ state. When $7b_2$ is populated, one gets a $^2B_2$ state in which the odd electron is shared by Li and Cl_2, *via* partial population of σ^*. The latter effect leads to an important charge transfer from Li to Cl_2. The relative energy of these two states obviously cannot be deduced from this analysis although the possibility of state crossing is strongly suggested. At infinite separation, $^2A_1$ is the most stable state. During the approach, an increasing destabilization of this state is found, while, at the same time, the stabilization of the $^2B_2$ state increases. Moreover, we see that the covalent excited state of Li obtained through population of its $2p_y$ AO plays a significant role in the overall process, along the $^2B_2$ potential energy surface.

A qualitative state correlation diagram is displayed in the lower part of Fig. 1. For the sake of simplicity, we have restricted ourselves to the three aforementioned potential energy surfaces (PESs), one of $^2A_1$ and two of $^2B_2$ symmetry, with our reference frame. At infinite separation (right), one finds in order of decreasing stability: (*i*) the covalent $^2A_1$ system composed of Li (^2S) and Cl_2 ($^1\Sigma_g^+$); (*ii*) at 1.84 eV above is found the covalent $^2B_2$(cov) state composed of excited Li (^2P) and Cl_2 ($^1\Sigma_g^+$); (*iii*) finally, we find the $^2B_2$ ionic charge transfer (CT) state, composed of Li^+ (^1S) and Cl_2^- ($^2\Sigma_u^+$), at 4.47 eV (MP2) or 4.64 eV (DFT) (see Table 1). As the partners approach from each other, both the $^2A_1$ (full lines) and $^2B_2$(cov) (dashed lines) states are destabilized due to the 3-electron repulsion arising, in each case, between the odd electron on Li and the doubly occupied MOs on Cl_2 of the same symmetry. In contrast, the $^2B_2$ (CT) state is stabilized (dashed lines). Both $^2B_2$ states cross at point P. In the vicinity of P, the odd electron has a strong possibility of jumping from the covalent PES to the ionic one. When the adiabaticity is taken into account, this crossing is avoided, thus yielding the full line behaviour for the two lowest energy PESs. The triangular complex that results contains a mixture of covalent and ionic $^2B_2$ states. Starting from infinite separation, the lowest energy state $^2A_1$ first reaches point Q through a weakly endothermic process. In the C_{2v} point group, an internal conversion is likely to take place at point Q since both PESs have different symmetries, but this is no longer the case as soon as a small deformation towards a C_s or $C_{\infty v}$ structure occurs, since in these new geometries both A_1 and B_2 symmetries yield a unique A′ (or Σ^+) irreducible representation. We also see that Cl_2 relation, which is endothermic in neutral Cl_2, is not likely to occur before point Q along the $^2A_1$ PES, so as to minimize the endothermic approach. The eventual Cl—Cl bond length relaxation will therefore take place along the $^2B_2$ PES, once the change of surface has occurred at point Q. The nature of the diabatic crossings occurring at points P and Q persists in any geometry.

Calculated MP2 PESs in the C_{2v} geometry

The lowest energy $^2A_1$ and $^2B_2$ PESs calculated in the C_{2v} geometry are reported in Fig. 2. They have been obtained by

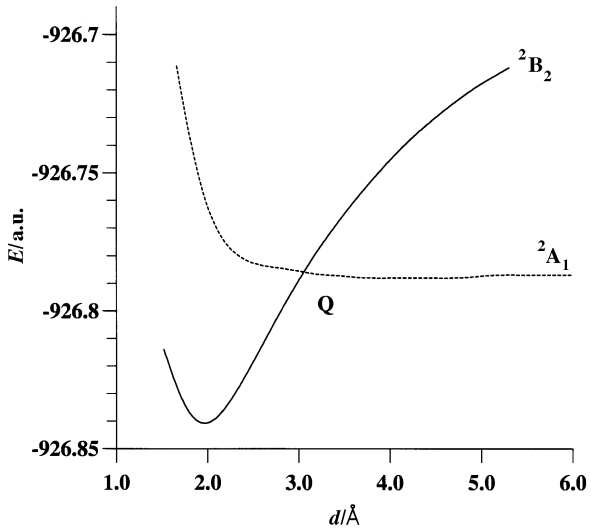

Fig. 2 Calculated PESs in the C_{2v} geometry. The $^2B_2$ PES has been obtained through a 'backward' process, that is starting from the left (see text), while the $^2A_1$ PES has been obtained through a 'forward' process, that is from right to left. The scanning of both PESs has been carried out with a constant increment of 0.14 Å

scanning *d* in increments of 0.14 Å. The $^2A_1$ PES has been obtained starting from a *long d* distance and then using the resulting initial SCF (self-consistent-field) MOs as guesses for decreasing *d* values (forward process). Conversely, the $^2B_2$ PES has been obtained by starting the calculation at a *short d* distance, and subsequent propagation of the resulting MOs as initial guesses for higher *d* values (backward process). Both results nicely confirm the analysis developed in Fig. 1. The PESs cross at point Q ($\approx$3 Å). A stable complex ($^2B_2$ symmetry) is obtained at $d = 1.94$ Å, lying 1.50 eV below the asymptotic neutral limit (Table 1). In this complex the spin density, calculated after the MP2 step, is 0.0192 on Li and 0.4904 on each Cl atom, thus showing that the electronic transfer is complete. The atomic charges, calculated at the MP2 level, are 0.6375 on Li and -0.3188 on Cl, showing that back-donation from the lone pairs of Cl_2^- towards Li^+ is present, *via* the $6b_2$ MO. Other studies have shown that upon complete structure optimization, one gets a true stable complex,[29–31] so that the situation that is reached through electron transfer might adiabatically evolve towards a more stable one, but this further evolution lies beyond the scope of the present study. These results show that two types of PESs, one covalent and one ionic, might be obtained in the region of diabatic crossing. It is noteworthy that a similar behaviour, not reported here for the sake of conciseness, is obtained when using the DFT/B3LYP or the CASSCF techniques.

Calculated PESs in the $C_{\infty v}$ and C_s geometries

In these geometries, both A_1 and B_2 irreducible representations of the C_{2v} point group, mix into a unique A′ or Σ^+ irreducible representation, respectively in the C_s or $C_{\infty v}$ geometry. The strong difference in the nature of the ionic and covalent PESs pointed out in the preceding paragraph persists, and strongly perturbates the SCF behaviour in the zones of the diabatic crossings. This is particularly striking for C_s geometries with $30° \leqslant \theta \leqslant 60°$. On the other hand, DFT calculations avoid this difficulty, and in Fig. 3(*A*) are displayed the calculated PESs corresponding to $\theta = 45°$ (C_s point group) and $\theta = 0°$ ($C_{\infty v}$ point group). It is noteworthy that in the linear geometry the stable complex is obtained at a larger distance than in the C_s geometry, though the actual distance between Li and the closest Cl atom lies in the same range in both cases. This results from our definition of the *d* parameter,

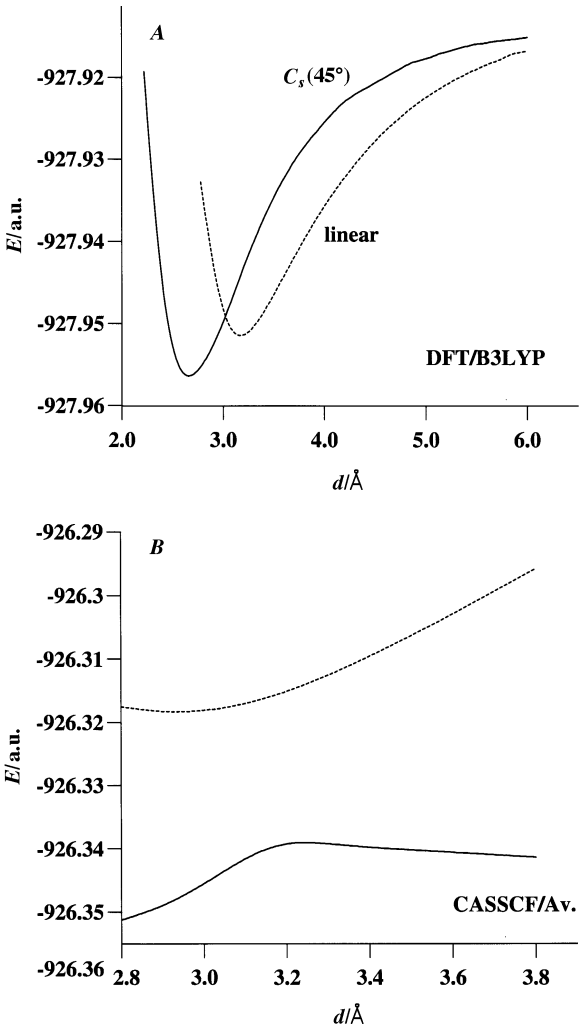

Fig. 3 (*A*) Calculated PESs in the $C_{\infty v}$ and C_s ($\theta = 45°$) geometries obtained with the DFT technique. (*B*) Zoomed display of the CASSCF/Average PESs of the two lowest states obtained for $\theta = 45°$ in the 2.8 Å $\leqslant d \leqslant$ 3.8 Å region

in which the origin is located at the midpoint of the Cl—Cl bond. With the DFT technique ($C_{\infty v}$ geometry), smooth PESs are obtained, but it is worth comparing the atomic charges and spin densities obtained with this method to those obtained by the MP2 method.

In a preliminary step, we have verified that both methods yield the same covalent species at long distances. The difference between both types of calculations is emphasized in Fig. 4, where the spin density (α spin) and atomic charge on Li are reported as a function of *d*, for the $C_{\infty v}$ geometry. On the one hand, one sees that both DFT curves show a progressive charge transfer process, with an already noticeable ionic character at 7 Å. On the other hand, the MP2 curves, which do not reveal any ionic character at $d = 7$ Å, undergo a drastic change in the region located around 4.5 Å. In Fig. 3(*B*) are reported the two lowest energy PESs of the C_s geometry, obtained at the CASSCF/Average/6-31G* level, for 2.8 Å $\leqslant d \leqslant$ 3.8 Å. In striking contrast with the behaviour of the DFT/B3LYP results of Fig. 3(*A*) we see that an avoided crossing between both PESs occurs in the 3.2 Å region. This finding is in better agreement with the previous study of Fig. 2. Since it was not our purpose to study the reason why the widely used DFT/B3LYP correlation yields such a continuous PES, a fundamental question is thus posed: which method gives the best description of the actual process? A possible answer would result in showing that, in reality, a *strong topological identity* lies beyond the apparent diversity coming from different

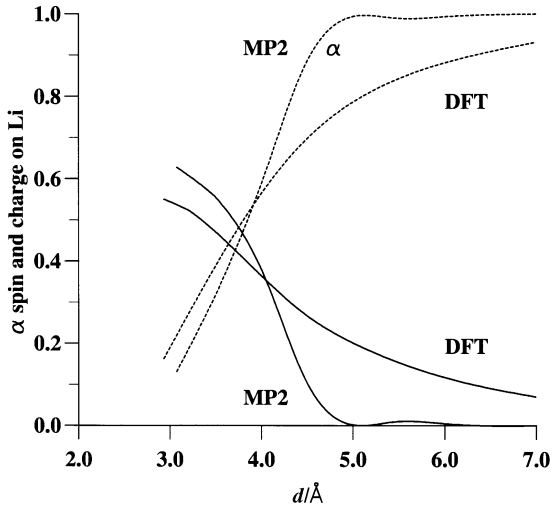

Fig. 4 Calculated atomic charge (solid lines) and spin density (α spin, dashed lines) on Li in the linear geometry from MP2 and DFT calculations

quantum mechanical calculations. This will be treated in the following sections.

BET Analysis

Bonding evolution theory, briefly presented in Appendix B, provides a description of the bonding features of a system, along with their evolution accompanying a reaction path. It relies on the variation of the ELF topological profile as a function of the nuclear coordinates. The ELF partitions the molecular space into open sets having a clear chemical meaning (see Appendix A) and corresponds to the classical chemists' vision of structures, in terms of bonds, lone pairs, *etc.* Obviously, this partition depends on the electronic state under scrutiny. In upcoming sections, we will first examine in detail the case of C_{2v} symmetry, using the MP2 results, keeping in mind that DFT and CASSCF calculations yield the same description. Then, the cases of $C_{\infty v}$ and C_s symmetries will be treated on the same grounds, though with slightly less detail, using the DFT and CASSCF results, respectively.

Electron transfer in the C_{2v} symmetry

Fig. 5 displays the C_{2v} molecular partition of the fragments for the three states previously discussed in the quantum mechanical section, at $d = 6$ Å. Fig. 5(*A*) and 5(*B*), respectively, display the $^2A_1$ and $^2B_2$ covalent states, and Fig. 5(*C*) shows the ionic $^2B_2$ charge transfer state. It is worth examining the striking features of the molecular partitions in each case. In the $^2A_1$ molecular partition, the disynaptic basin V(Cl1, Cl2) indicated by an arrow, corresponds to the Cl—Cl bond.[32] Two basins are found around Li, one corresponding to its core C(Li), and the second one, V(Li), to its valence odd electron (L shell). The $^2B_2$ covalent state is characterized by two monosynaptic basins, V1(Li) and V2(Li), located on both sides of the C(Li) basin in the molecular plane. They correspond to the half-filled 2p AO of Li. As when dealing with the previous state, the Cl atoms are bonded through a disynaptic basin, still noted V(Cl1, Cl2). In the ionic state, the Cl atoms are linked by a (3, −1) saddle point, or alternatively by a critical point of index $I = 1$ (see Appendix C), typical of a 3-electron bond. Around Li, one only finds the core basin C(Li). In all three states, the valence electrons of the Cl lone pairs are contained in a torus centred on the atom and perpendicular to the Cl—Cl axis.

Fig. 6(*A*) displays the molecular partition of the short distance complex. Between both Cl atoms there exists a (3, −1)

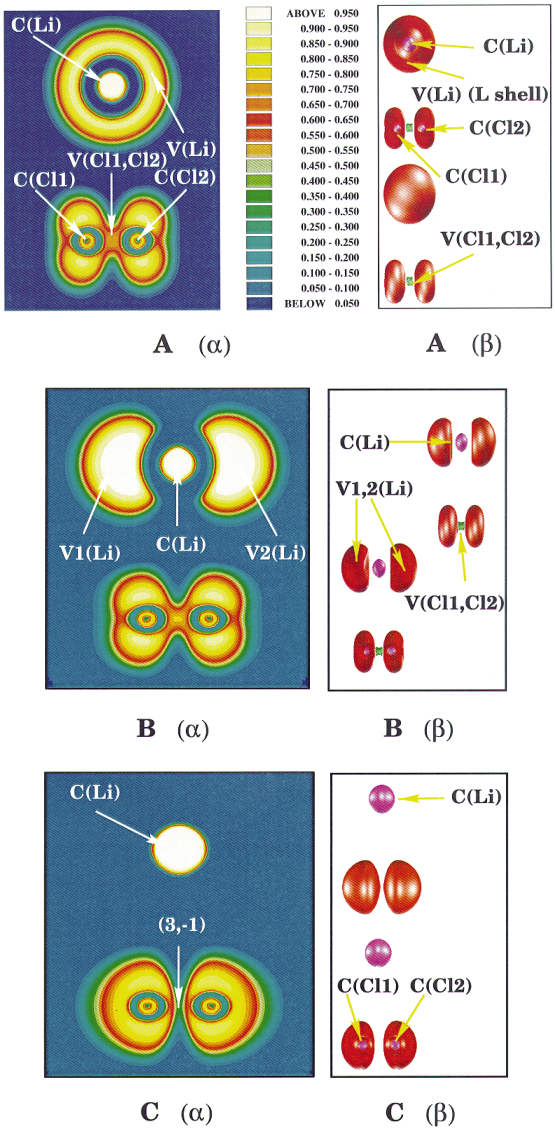

Fig. 5 (*A*) The ELF molecular partition of the $^2A_1$ state in the C_{2v} geometry, $d = 6.00$ Å. (α) The projection of the ELF onto the molecular plane. (β) Upper: Cut of the ELF isosurface ($\eta = 0.8$). Lower: Entire envelope of the same ELF isosurface. (*B*) The same as (*A*) for the $^2B_2$ state. (*C*) The same as (*A*) for the charge transfer state

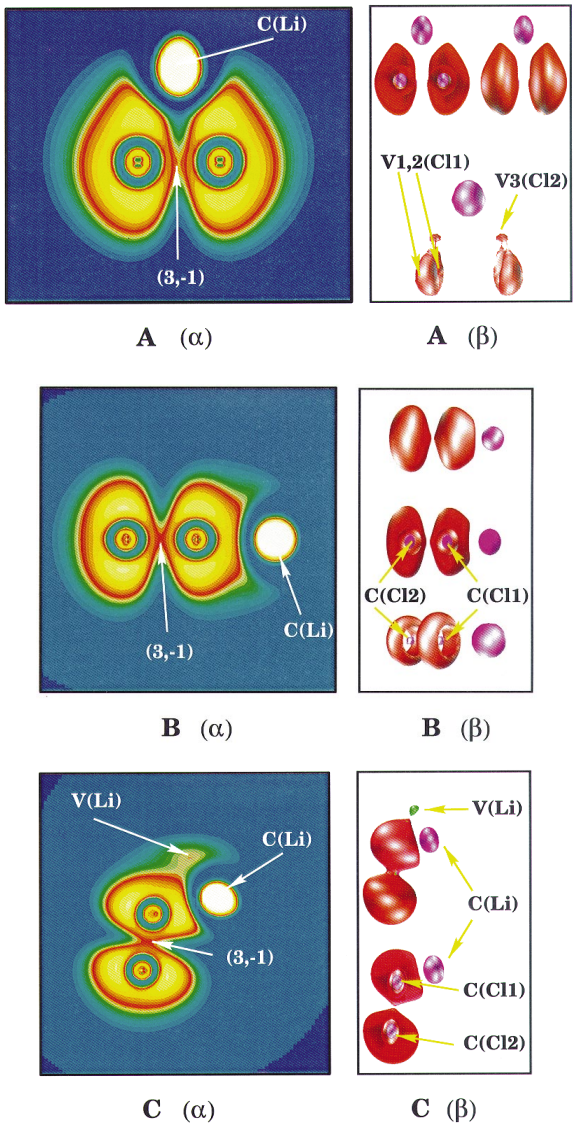

Fig. 6 (*A*) The ELF partition of the C_{2v} complex defined in Table 1 (MP2 calculations). See Fig. 5 for an explanation of the various parts of the figure. (*B*) Same as (*A*) for the $C_{\infty v}$ complex (DFT/B3LYP) calculations). (*C*) Same as (*A*) for the C_s ($\theta = 45°$) complex (CASSCF/MP2 calculations)

critical point, and each Cl valence torus now splits into three basins. Two of them, labelled V1(Cl*i*) and V2(Cl*i*) ($i = 1, 2$), are located on both sides of the molecular plane, while the third one, labelled V3(Cl*i*), lies in the molecular plane and is directed towards Li. This structure might be considered as a mixture of both covalent and ionic $^2B_2$ states, in which V3(Cl1) and V3(Cl2) are remnants of the V1(Li) and V2(Li) basins found at large distance, Fig. 5(*B*). It is noteworthy that the presence of a (3, −1) critical point between both Cl atoms might be related to the existence of a 3-electron bond, which is well-documented for the Cl_2^- species.

In Fig. 7, a schematical description of the reaction, yielding the previously examined complex, is displayed as a function of the control parameter *d*. The crossing at point **Q**, previously described in Fig. 1, is first studied. It takes place at $d = 3.06$ Å. For both crossing states, the ELF η has been calculated. At **D**, the structure of the $^2A_1$ state is given. The slightly polarized V(Li) and the C(Li) basins are shown, along with the still existing V(Cl1, Cl2) basin. **E** shows the $^2B_2$ ionic state at point Q. As expected, there is no common topological feature between **D** and **E**, in agreement with the fact that both states

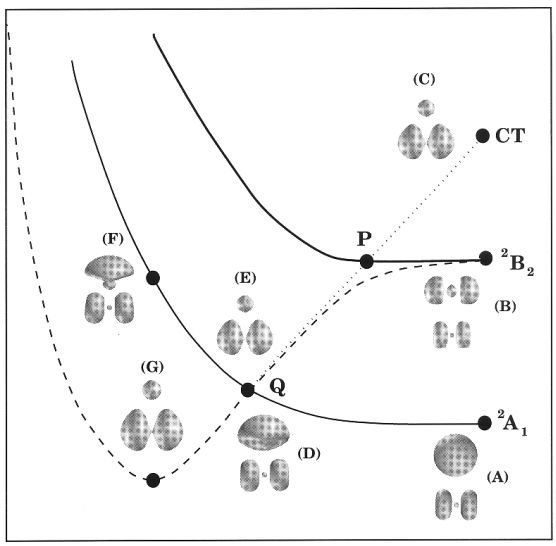

Fig. 7 Display of the ELF for various values of *d* in the C_{2v} geometry, calculated with the TopMoD series of programs (same coordinates as in Fig. 2)

have different symmetries. Let us now focus our attention on the $^2B_2$ state (**E**). By comparison with **C**, one sees that the latter state is mostly ionic, thus showing that a crossing with the steeply descending CT state has already occurred. As in Fig. 1, this crossing point is noted P. The BET method has been used for localizing the avoided crossing at point P. Adiabatic calculations, starting from $d = 6.00$ Å, have been carried out along the covalent $^2B_2$ PES. For 4.88 Å $< d \leqslant 6$ Å, all molecular partitions are equivalent to the one at **B** [or Fig. 5(*B*) as well], thus showing that the system lies in a region of structural stability (see Appendix D).

At $d^* = 4.88$ Å, and within a narrow range ($\approx$0.12 Å), three catastrophes occur quite simultaneously. The first catastrophe corresponds to the breaking of the Cl—Cl bond. The disynaptic basin V(Cl1, Cl2) of the covalent Cl—Cl bond yields two monosynaptic ones and a (3, −1) saddle point. After this catastrophe, a reorganization of the electron the C1 cores takes place, which splits the valence basins of the Cl atoms into two basins, V1(Cl*i*) and V2(Cl*i*) ($i = 1, 2$). The latter process has no great importance in the scope of localizing the crossing itself. The second and third catastrophes involve the V1(Li) and V2(Li) basins and correspond to the harpooning process; the electronic density they contain [Fig. 7, **B** or Fig. 5(*B*)] is absorbed by the Cl valence basins. Once this process has occurred, the system remains topologically equivalent to the complex of Fig. 6(*A*).

Another interesting feature is the evolution of the CT state, in going from large distance to point P. In the vicinity of point P, the two torus basins of the Cl atoms split, yielding the two additional small basins of Fig. 6(*A*), labelled V3(Cl1) and V3(Cl2), directed towards Li^+ along both Cl—Li axes. The latter behaviour corresponds to the back-donation mentioned in the discussion of Fig. 1. The integration of the electronic density within the basins of a molecular partition yields their population. The calculated results are given in Table 2. The aforementioned changes in the topology exactly reveal the crossing of the CT and of the $^2B_2$ covalent PESs. The existence of the crossing at point Q explains the ionic nature of the complex at its equilibrium distance [Fig. 7, **G** or Fig. 6(*A*)]. In conclusion, BET allows the avoided crossings to be localized by comparing the topology of the complex to that of the asymptotic species. Moreover, when the crossing is symmetry-allowed, it preserves the symmetry of the crossing states.

Electron transfer in the $C_{\infty v}$ and C_s symmetries

In both symmetries, we have kept the same definition of the parameter d as in the C_{2v} geometry. In the C_s symmetry, only the value of $\theta = 45°$ has been considered in detail. For both $C_{\infty v}$ and C_s situations, the topology of η has been examined along the reaction path for $d_c \leqslant d \leqslant 6.00$ Å, where d_c is the value corresponding to the stable complexes, that is, 3.14 Å [DFT, $C_{\infty v}$, Fig. 6(*B*)] and 2.71 Å [CASSCF, C_s, Fig. 6(*C*)]. As previously found in the C_{2v} geometry, these complexes are also characterized by the absence of the disynaptic basin V(Cl1, Cl2), and by the fact that, around Li, there is only one core basin C(Li), indicating a complete electron transfer from Li to Cl_2.

Fig. 8 shows the evolution of molecular partition in the linear $C_{\infty v}$ symmetry, along the reaction path. **A** displays the fragment topology at $d = 6.00$ Å, which exhibits the same features as in the corresponding situation in the C_{2v} geometry. Around $d^* \approx 4.75$ Å one finds a turning point, the corresponding molecular partition is shown in **Bα** ($\eta = 0.75$) and **Bβ** ($\eta = 0.5$). This bifurcation state corresponds to the breaking of the V(Cl1, Cl2) disynaptic basin, which yields two monosynaptic basins and a (3, −1) saddle point between them. This topological shift indicates the existence of a diabatic crossing between the lowest energy covalent PES and a descending state having a strong ionic character. After this crossing, the system remains ionic.

The ELF representation of the $C_{\infty v}$ complex is displayed in Fig. 6(*B*) where the Li atom is restricted to its core basin, indicating that the electron transfer is complete. The population of the basins of the complexes, in different situations, is given in Table 2. The electron transfer in C_s geometries is characterized by the same features as in C_{2v} and $C_{\infty v}$ symmetries. It is noteworthy that in the C_s geometry, the 'topological memory' of the covalent asymptotic state that remains after the crossing is more easily understood by examination of the complex structure in Fig. 5(*C*) ($\theta = 45°$), in which a weakly populated V(Li) basin subsists under the same conditions.

Modelization of the process

In all cases, the avoided crossings are associated with the topological changes accompanying the chemical transformation, that is, the breaking of the Cl—Cl bond that takes place at a particular d^* value of the control parameter, in the molecular partition of the starting configuration. More precisely, the *dual cusp* catastrophe that characterizes the breaking of a covalent bond[19] involves the V(Cl1, Cl2) attractor located at $\mathbf{r}^{(c)}$. The Taylor development of $\eta(\mathbf{r}; d)$, around $\mathbf{r}^{(c)}$, after a change of variables can be written as:[33]

$$\eta(x, a, b) \doteq -[\tfrac{1}{4}x^4 + \tfrac{1}{2}a(d \text{ or } \theta)x^2 + b(d \text{ or } \theta)x] \qquad (1)$$

(see Appendix D for the meaning of $\doteq$). In this equation, x is a generalized space variable along the Cl—Cl axis.

The threefold degenerate critical point, $\mathbf{r}^{(c)}$, which is obtained for $a = b = 0$, is located at the origin $x = 0$, the midpoint of the Cl—Cl bond. The observed topological behav-

Table 2 Basin populations of the complexes

	C_{2v}	$C_{\infty v}$	C_s ($\theta = 45°$)
C(Cl1)	10.07	10.06	10.07
C(Cl2)	10.07	10.06	10.08
C(Li)	2.03	2.02	2.02
V(Li)			0.1
V_t(Cl1)	7.40	7.61	7.47
V_t(Cl2)	7.40	7.23	7.24

V_t(Cl*i*) with $i = 1, 2$ means the total valence population of the Cl atoms.

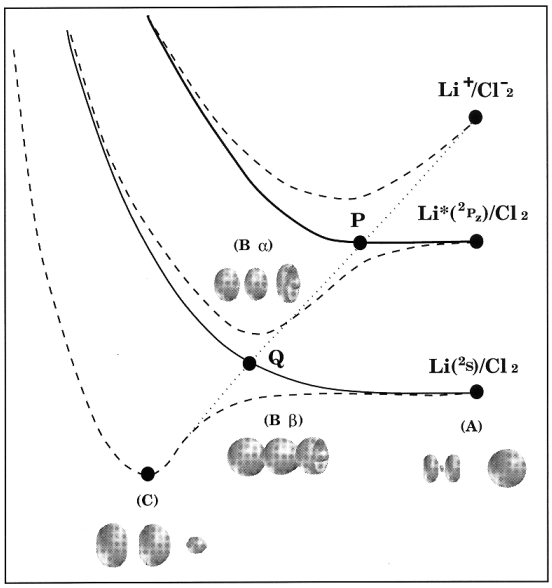

Fig. 8 Display of the ELF for various values of d in the $C_{\infty v}$ geometry, calculated with the TopMoD series of programs

iour, for example in C_{2v} symmetry, implies that b is constant during the process, and equal to the value found for the bifurcation state. Accordingly, in the latter equation, $b(\theta) = b^*(\theta)$ is determined by the condition for which x_0, which locates the attractor Cl—Cl bond for a given θ, becomes triply degenerate:[33]

$$\left.\frac{d\eta}{dx}\right|_{x_0} = \left.\frac{d^2\eta}{dx^2}\right|_{x_0} = 0 \qquad (2)$$

This condition yields $b(\theta) = 2x_0^3$.

For the corresponding value of a, namely $a(d^*)$, one gets $a(d^*) = -3x_0^2 = [-\frac{27}{4}b^2(\theta)]^{1/3}$. Hence, the splitting of the V(Cl1, Cl2) basin takes place as $a(d)$ passes from $a(d) > a(d^*)$ to $a(d) < a(d^*)$, *via* $a(d) = a(d^*)$. The latter finding means that, for $a(d^*)$, either the attractor (in the C_{2v} symmetry), or in other cases, a wandering point of the V(Cl1, Cl2) basin, that is, a point that satisfies the condition $\nabla_{\mathbf{r}}\eta \neq 0$, becomes degenerate, with one zero eigenvalue. Then, after a small perturbation, expressed by a, and corresponding to a variation of d, two monosynaptic basins and a (3, −1) saddle point between them appear. The C_{2v} symmetry implies that $b(90°) = 0$, while for other values of θ, $b(\theta) \neq 0$, which describes the disymmetry of the bond breaking.

Fig. 9 displays the partition of the control space, according to the number of maxima (full circles) and saddle points (full triangles) of the η function. Regions I.1 and II.1 correspond to the molecular partitions in which the V(Cl1, Cl2) basin exists (one maximum), while regions I.2 and II.2 correspond to molecular partitions in which the Cl—Cl bond is broken [two maxima and a (3, −1) saddle point]. The domains having $b < 0$ and $b \geqslant 0$ differ by the way the θ angle is defined. In the present study, only the case $b \geqslant 0$ has been explored; the case $b > 0$ corresponds to a symmetrical definition of θ. Thus, the electron transfer is considered as a trajectory in the control space, in the sense described above. The cusp curve represents the transitions from region I.1 to I.2, and characterizes the avoided PES crossings.

Comparison with a classical model

A very simple qualitative model, using the point charge approximation[1] and either MP2 or DFT calculated data at infinite separation, may be used for determining the region and nature of the electronic events corresponding to the critical points of the system, depending on the variable d, at constant θ. Let us take the neutral covalent system $\{Li(^2S) + Cl_2(^1\Sigma_g^+)\}$, at infinite separation of both partners, as the energy reference: $E_{cov} = 0$. The ionic charge transfer (CT) system composed at $d = \infty$ of $\{Li^+(^1S) + Cl_2^-(^1\Sigma_u^+)\}$ lies

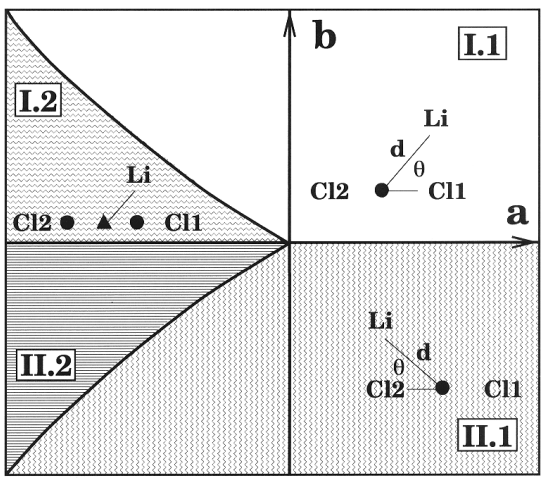

Fig. 9 Partition of the control space according to the number of maxima and saddle points in the η function[39]

4.47 eV (MP2) or 4.64 eV (DFT) higher (the CT energy is noted E_{ion}). Upon the assumption that the CT energy varies according to a $-d^{-1}$ law, one straightforwardly gets the following equation, which links the parameter d (in Å), the CT energy and the actual energy under scrutiny, noted E (in eV)

$$d = \frac{14.4}{E_{ion} - E} \qquad (3)$$

The critical regions, corresponding to a crossing between the CT and a covalent PES are then obtained by equating E to the discrete spectra of the various states of the neutral $\{Li + Cl_2\}$ system in this expression. This rough approximation relies on the implicit statement that the actual overlap between the frontier MOs of both partners remains small in the regions of crossing, in such a way that no strong MO interaction results. We thus obtain two regions of interest. With the MP2 data, one gets the following critical regions: (*i*) the first one concerns the crossing of the CT PES with the $\{Li(^2P) + Cl_2(^1\Sigma_g^+)\}$ covalent PES, at point P, located around 5.5 Å; (*ii*) the second one concerns the crossing of the CT PES with the $\{Li(^2S) + Cl_2(^1\Sigma_g^+)\}$ PES, at point Q ≈ 3.2 Å. Under the same conditions the DFT data yields 3.1 Å for point Q and 5.1 Å for point P. We thus see that both types of calculations give comparable results. Moreover, the very simple model whose physical signification is quite evident, is in very good agreement with the BET results, thus showing that the latter have a firm chemical signification and provide qualitatively the same description of the actual process at all quantum mechanical levels of calculation.

Conclusions

In a context of *irreversible* conditions, electron transfer in the $\{Li + Cl_2\}$ system realizes and illustrates the intuitive knowledge we have of a 'catastrophic decay'. When Li and Cl_2 approach each other in the C_{2v} geometry, which is the simplest reference for any discussion, we observe a crossing between the covalent PES of the neutral ground state and the ionic $\{Li^+ + Cl_2^-\}$ CT PES. Through this crossing, an electron jump takes place from the covalent to the ionic PES, with a probability that can be estimated by the classical Landau–Zener model.[14] In the usual adiabatic description this crossing becomes more or less avoided in any other geometry, for symmetry reasons,[13] though offering the possibility of a progressive electron transfer, but the question might be raised of the pertinence of this result. In particular, once the electron has been trapped by Cl_2 to form a 3e-bond, stable at all Cl—Cl distances, an irreversible further chemical evolution gives LiCl + Cl *via* a strongly exothermic process. It is therefore difficult to speak in terms of a potentially reversible process in this case, and the diabatic language seems more appropriate.

The topological analysis of ELF η, either based on the calculated MP2, DFT or CASSCF results, nicely confirms this analysis by providing a firm basis for a topological analysis of the electronic events, in the general catastrophe theory framework. It thus becomes possible to identify the invariant corresponding to this type of process, namely a dual cusp, whose universal unfolding variable might easily be related to the actual geometrical constraints. After the resulting general modelization, it becomes possible to find the crossing zone in any geometry. The topological study presented here illustrates the fact that, although a smooth continuous PES profile might be afforded in some cases, it is possible to extract the 'memory' of the diabatic crossings occurring in any geometry and detected through the existence of the dual cusp catastrophe. This type of investigation, which, as shown by our study, is largely method-independent will be developed by further studies of various irreversible processes.

Appendices

Appendix A: Electron localization function (ELF)

The first topological approach to bonding was made by Richard Bader in his atoms-in-molecules theory, in which he applied topological concepts to the electronic density $\rho(\mathbf{r})$.[16] The unstable manifold of the (3, −1) critical points constitutes the bond path that links the bonded centres together (see Appendix C). Apart from structure considerations, this theory has been applied to unimolecular reactions and dissociative processes. In the most general case of bond dissociation, the study of the electronic density does not allow any change in the structure of attractors to be identified, with the exception of systems possessing a non-nuclear attractor, such as Li_2.[34] In order to illustrate this, let us consider the bond breaking of a singly bonded diatomic molecule. In this case, the unique control parameter is the internuclear distance, and there always exists a (3, −1) critical point between both attractors, in such a way that the system always remains structurally stable (see Appendix D): nothing seems to happen.

Bonding evolution theory (see Appendix B), provides an alternative method for classifying and studying chemical processes that overcomes the previous inconveniency. It is based on the Silvi and Savin[17] description of bonding, resulting from the topological analysis of Becke and Edgecombe's ELF.[20] The latter function is defined by

$$\eta(\mathbf{r}) = \frac{1}{1 + \left(\frac{D(\mathbf{r})}{D_h(\mathbf{r})}\right)^2} \quad \text{(A1)}$$

For a single determinant wavefunction built from orbitals labelled ϕ_i, the quantity $D(\mathbf{r})$ defined according to:

$$D(\mathbf{r}) = \frac{1}{2}\sum_i |\nabla\phi_i(\mathbf{r})|^2 - \frac{1}{8}\frac{|\nabla\rho(\mathbf{r})|^2}{\rho(\mathbf{r})} \quad \text{(A2)}$$

is the excess of local kinetic energy, due to Pauli's repulsion.[35] $D_h(\mathbf{r}) = C_F\,\rho(\mathbf{r})^{5/3}$ is the Thomas–Fermi kinetic energy density, which acts here as a renormalization factor, and C_F is the Fermi constant ($C_F = 2.871$ a.u.). The range of values of η is $0 \leqslant \eta \leqslant 1$. For a single pair of electrons with antiparallel spins, $\eta = 1$, while for a uniform gas of electrons, by construction, $\eta = 0.5$.

In principle, the ELF can be calculated from the exact wavefunction, if available, or from experimental results. In practice $\eta(\mathbf{r})$ is calculated from the *natural orbital populations*, with no restriction on the quantum mechanical method used for obtaining them. In the Silvi–Savin theory of bonding, a partition of the molecular space into basins of attractors having a clear chemical signification is obtained. These basins are either *core* basins located around the nuclei with $Z \geqslant 2$, or *valence* basins, some of which are associated with bonds. In this context, a classification of bonds has been proposed.

Appendix B: Main features of bonding evolution theory (BET)

This theory consists of a set of topological concepts characterizing the chemical changes taking place along a reaction path. These concepts, by nature, are independent of the actual quantum mechanical method used for calculating the ELF. Accordingly, BET is compatible with any quantum mechanical scheme. Moreover, the topological description of a process is structurally stable, in the sense that the number and type of critical points of the ELF, as well as their connectivity and evolution, remain constant for any quantum method yielding a wavefunction that suitably describes the system in any configuration. To distinguish the valence basins among themselves, the concept of a *synaptic order* σ has been introduced.[32] This is the number of core basins with which a given valence basin shares a common boundary, as shown in Table B1. From a chemical point of view, monosynaptic basins are related to lone pairs, while di- and polysynaptic basins are related to bonds. In terms of BET,[19] a chemical process is considered as a succession of different regions of structural stability in the control space (the space of nuclear coordinates) passing through a *bifurcation state* (see Appendix D). BET introduces the concept of *morphic number* μ, as being the number of basins of the molecular partition of the system[19] in each region of structural stability. It generalizes the molecular graph concept (Appendix C), first introduced by Bader.[16] By definition, a step in a chemical process takes place when a change occurs in the topological structure of the gradient field of the ELF associated with the system. The latter changes are typical of physical or chemical events such as bond breaking and forming, or of an electron switch from one PES to another, around a conical intersection. This approach provides a classification of chemical processes according to topological arguments. It is worth recalling that this classification is likely to remain independent of the quantum chemical method that is used for obtaining the PESs.

Table B1 Nomenclature of valence basins

Synaptic order σ	Nomenclature	Symbol
0	Asynaptic	V
1	Monosynaptic	V(X*i*)
2	Disynaptic	V(X*i*, X*j*)
$\geqslant 3$	Polysynaptic	V(X*i*, X*j*, …)

The expression in parenthesis corresponds to the list of core basins sharing a common boundary with the valence basin under scrutiny.

Appendix C: Topological concepts

The gradient field of a local, well-defined function, $F(\mathbf{r}; c_\alpha)$, may be considered as a velocity vector field, as shown by the following relation:

$$\frac{d\mathbf{r}}{d\tau} = \nabla_{\mathbf{r}} F(\mathbf{r}; c_\alpha) \quad \text{(C1)}$$

This corresponds to a system of equations, which is called a *gradient dynamical system.*[36] In any such equation τ is an effective time and c_α represents the set of control parameters that $F(\mathbf{r}; c_\alpha)$ depends on. In our case, c_α is the set of nuclear coordinates. Integration of the previous equation, with respect to some initial conditions, yields a unique solution, which is a trajectory, $\mathcal{R}^3$. For a given trajectory, the points corresponding to $\tau \to -\infty$ and $\tau \to +\infty$ are called the $\alpha - limit$ and $\omega - limit$, respectively. The set of $\omega -$ limits is the set of attractors of the gradient dynamical system. The basin of an attractor is the set of points for which this attractor is the $\omega -$ limit. The set of trajectories having a given critical point as $\alpha -$ limit is called the *unstable manifold* of the critical points, whereas the *stable manifold* is defined as the set of trajectories for which it is the ω limit.

The points for which $\nabla_{\mathbf{r}} F(\mathbf{r}; c_\alpha) = 0$ are of particular importance. They are called *critical points* and are characterized by the couple (r, s) formed by the rank r, which is the number of non-zero eigenvalues, and the signature s, which is the excess of positive eigenvalues of the *Hessian matrix*, the elements of which are the second derivatives of $F(\mathbf{r}; c_\alpha)$. In $\mathcal{R}^3$, a critical point of $\mathbf{r} = 3$ is called *non-degenerate*, and according to the signature, four types of critical points are distinguished: (*i*) (3, −3), attractor; (*ii*) and (*iii*) (3, +1) and (3, −1), saddle points; (*iv*) (3, +3), repellor. Alternatively, a critical point is characterized by its index I, which is the number of positive eigenvalues of the Hessian matrix, calculated at the critical point, labelled $\mathbf{r}^{(c)}$. With this definition, an attractor corresponds to $I = 0$, a repellor to $I = 3$, while the saddle points (3, +1) and (3, −1)

Table D1 Thom's nomenclature of elementary catastrophes

Name	Codimension	Corank	Universal unfolding
Fold	1	1	$x^3 + ux$
Cusp	2	1	$x^4 + ux^2 + ux$
Swallow Tail	3	1	$x^5 + ux^3 + vx^2 + wx$
Hyperbolic Umbilic	3	2	$x^3 + y^3 + uxy + vx + wy$
Elliptic Umbilic	3	2	$x^3 - xy^2 + u(x^2 + y^2) + vx + wy$
Butterfly	4	1	$x^6 + ux^4 + ux^3 + wx^2 + tx$
Parabolic Umbilic	4	2	$x^2y + y^4 + ux^2 + vy^2 + wx + ty$

correspond to $I = 2$ and $I = 1$, respectively. These critical points satisfy the Poincaré–Hopf relationship[36]

$$\sum (-1)^I \mathbf{r}^{(c)} = 1 \text{ for finite systems, and}$$

$$0 \text{ for periodic systems} \quad \text{(C2)}$$

In the previous equation, the sum runs over all critical points of the gradient dynamical system. In bonding evolution theory, the critical points form the *molecular graph*. In this graph, they are represented according to the dimension of their unstable manifold. Thus, critical points of $I = 0$ are associated with a dot, those with $I = 1$ are associated with a line, those with $I = 2$ by faces, and finally those with $I = 3$ by 3D cages.

Appendix D: Elements of catastrophe theory

Catastrophe theory[37] studies the change of the critical points $[(\mathbf{r}^{(c)}; c_\alpha)$, see Appendix C] of a gradient dynamical system as a function of the changes of the control parameters c_α, in the special case where the dimension k of the control space W, also called the *codimension*, fulfills the relationship: $k \leqslant 4$. In this context, the evolution of the critical points can be studied by considering the behaviour of the Hessian matrix H of $F(\mathbf{r}; c_\alpha)$ (see Appendix C). The configuration of the control parameters c_α^* for which the determinant of H is zero, that is $\det H_{ij}(c_\alpha^*)|_{\mathbf{r}=\mathbf{r}^{(c)}} = 0$ is called a *bifurcation state*. The set of c_α for which the Hessian matrix of a given critical point is non-zero defines the *domain of stability* of the critical point. A small perturbation of $F(\mathbf{r}; c_\alpha^*)$ brings the system from one domain of stability to another one. If none of the critical points of the system change during a variation of c_α, the system is located in a *domain of structural stability*.

Thom's theorem[37] states that in the neighborhood of $(\mathbf{r}^{(c)}; c_\alpha^*)$, after a smooth change of the variables, the function F can be written in the form: $F(\mathbf{r}; c_\alpha) \doteq Q + u$ where $\doteq$ means 'equal after a smooth change of variables'. In this equation, u is the *universal unfolding* of the singularity, it is a polynomial function of degree higher than 2 of a canonical form. The latter polynomial depends on l variables associated with the l zero eigenvalues of the Hessian matrix. l is called the *corank*, while Q is a quadratic expression of the $r - l$ variables, r being the rank of the Hessian matrix. The unfolding contains all the information about how $F(\mathbf{r}; c_\alpha)$ may change around the critical point when the control parameters change. Thom has classified these universal unfoldings according to their corank and codimension, as reported in Table D1.

References

1 D. R. Herschbach, in *Reactive Scattering in Molecular Beams*, Advances in Chemical Physics Series, Wiley, Chichester, 1966, vol. 10, p. 319.
2 H. C. Loguet-Higgins and E. W. Abrahamson, *J. Am. Chem. Soc.*, 1965, **87**, 2045.
3 (*a*) R. B. Woodward and R. Hoffmann, *J. Am. Chem. Soc.*, 1965, **87**, 2046; (*b*) K. Fukui, *Tetrahedron Lett.*, 1965, 2009.
4 (*a*) D. M. Silver, *J. Am. Chem. Soc.*, 1974, **96**, 5959; (*b*) D. Grimbert and L. Salem, *Chem. Phys. Lett.*, 1976, **43**, 435.
5 R. B. Woodward and R. Hoffmann, in *The Conservation of Orbital Symmetry*, Verlag Chemie, Weinheim, 1970.
6 L. Salem, *J. Am. Chem. Soc.*, 1974, **96**, 3486.
7 L. Salem, W. G. Dauben and N. J. Turro, *J. Chim. Phys. Phys. Chim. Biol.*, 1973, **70**, 694.
8 W. G. Dauben, L. Salem and N. J. Turro, *Acc. Chem. Res.*, 1975, **8**, 41.
9 A. Devaquet, A. Sevin and B. Bigot, *J. Am. Chem. Soc.*, 1978, **100**, 2009.
10 (*a*) B. Bigot, A. Sevin and A. Devaquet, *J. Am. Chem. Soc.*, 1979, **101**, 1095; (*b*) *ibid.*, 1979, **101**, 1101.
11 E. M. Evleth and A. Sevin, *J. Am. Chem. Soc.*, 1981, **103**, 7414.
12 (*a*) A. Sevin, *Nouv. J. Chim.*, 1981, **3**, 233, (*b*) A. Sevin and P. Chaquin, *Nouv. J. Chim.*, 1983, **7**, 353.
13 L. Salem, C. Leforestier, G. Segal and R. Wetmore, *J. Am. Chem. Soc.*, 1975, **97**, 479.
14. (*a*) E. E. Nikitin, in *Theory of Atomic and Molecular Processes in Gases*, Oxford University Press, Oxford, 1974; (*b*) E. E. Nikitin, *J. Chem. Phys.*, 1965, **43**, 744; (*c*) A. Bjerre and E. E. Nikitin, *Chem. Phys. Lett.*, 1967, **1**, 179; (*d*) J. B. Delos and W. R. Thorson, *Phys. Rev. A*, 1973, **6**, 728; (*e*) C. A. Mead and D. G. Truhlar, *J. Chem. Phys.*, 1982, **77**, 6090; (*f*) M. Desouter Lecomte, D. Dehareng and J. C. Lorquet, *J. Chem. Phys.*, 1987, **86**, 1429 and references cited therein.
15 (*a*) P. Chaquin, A. Sevin and H. T. Yu, *J. Phys. Chem.*, 1985, **89**, 2813; (*b*) A. Sevin, P. C. Hiberty and J. M. Lefour, *J. Am. Chem. Soc.*, 1987, **109**, 1845; (*c*) P. Chaquin and A. Sevin, *Chem. Phys.*, 1988, **110**, 5681; (*e*) P. Chaquin A. Sevin and A. Papakondylis, *Chem. Phys.*, 1990, **143**, 39; (*f*) P. Chaquin, A. Papakondylis, C. Giessner-Prettre and A. Sevin, *J. Phys. Chem.*, 1990, **94**, 7352; (*g*) A. Sevin, P. Chaquin and A. Papakondylis, *Chem. Phys. Lett.*, 1990, **174**, 185; (*h*) A. Sevin, C. Giessner-Prettre, P. C. Hiberty and E. Noizet, *J. Phys. Chem.*, 1991, **95**, 8480.
16 R. F. Bader, in *Atoms in Molecules: A Quantum Theory*, Oxford University Press, Oxford, 1990.
17 B. Silvi and A. Savin, *Nature* (*London*), 1994, **371**, 683.
18 T. S. Slee, *J. Am. Chem. Soc.*, 1986, **108**, 7541.
19 X. Krokidis, S. Noury and B. Silvi, *J. Phys. Chem.*, 1997, **101**, 7277.
20 A. D. Becke and K. E. Edgecombe, *J. Chem. Phys.*, 1990, **92**, 5397.
21 M. J. Frisch, G. W. Trucks, H. B. Schlegel, P. M. W. Gill, B. G. Johnson, M. A. Robb, J. R. Cheeseman, T. Keith, G. A. Peterson, J. A. Montgomery, K. Raghavachari, M. A. Al-Laham, V. G. Zakrezewski, J. V. Ortiz, J. B. Foresman, J. Cioslowski, B. B. Stefanov, A. Nanayakkara, M. Challacombe, C. Y. Peng, P. Y. Ayala, W. Chen, M. W. Wong, J. L. Andres, E. S. Replogle, R. Gomperts, R. L. Martin, D. J. Fox, J. S. Binkley, D. J. Defree, J. Baker, J. P. Stewart, M. Head-Gordon, C. Gonzalez and J. A. Pople, *Gaussian 94*, *Revision C3*, Gaussian Inc., Pittsburg, PA, 1995.
22 M. Dupuis, A. Marquez and E. R. Davidson, *HONDO 95.6*, IBM Corp., Kingston, NY, 1995.
23 P. M. Kozlowski and E. R. Davidson, *J. Chem. Phys.*, 1994, **100**, 3672.
24 H. J. Werner and W. Meyer, *J. Chem. Phys.*, 1981, **74**, 5894.
25 D. M. Hirst, *Adv. Chem. Phys.*, 1982, **50**, 517.
26 M. M. Francl, W.J. Pietro, W. J. Hehre, J. S. Binkley, M. S. Gordon, D. J. De Frees and J. A. Pople, *J. Chem. Phys.*, 1982, **77**, 3654 and references cited therein.
27 S. Noury, X. Krokidis, F. Fuster and B. Silvi, *TopMoD Series of Programs*, 1997. This software is available upon request at the following e-mail address: Xenophon.Krokidis@lct.jussieu. fr.
28 (*a*) T. V. Hertel, *Adv. Chem. Phys.*, 1981, **45**, 341; (*b*) T. V. Hertel, *Adv. Chem. Phys.*, 1982, **50**, 475; (*c*) W. H. Breckenridge and H. Umemoto, *J. Chem. Phys.*, 1981, **75**, 698; (*d*) W. H. Breckenridge and H. Umemoto, *J. Chem. Phys.*, 1981, **75**, 4153; (*e*) R. P. Blickensderfer, K. D. Jordan, N. Adams and W. H. Breckenridge, *J. Phys. Chem.*, 1982, **86**, 1930; (*f*) W. H. Breckenridge and H. Umemoto, *Adv. Chem. Phys.*, 1982, **50**, 325.

29 F. Ramondo, N. Sanna and L. Bencivenni, *J. Mol. Struct.* (*THEOCHEM*), 1992, **258**, 361.
30 J. Guan-Zhi and E. R. Davidsen, *J. Phys. Chem.*, 1992, **96**, 3683.
31 F. B. C. Machado, J. Guan-Zhi and E. R. Davidson, *J. Phys. Chem.*, 1997, 97, 5882 and references cited therein.
32 A. Savin, B. Silvi and F. Colonna, *Can. J. Chem.*, 1986, **74**, 1088.
33 (*a*) T. Poston and P. N. Stewart, in *Taylor Expansion and Catastrophes*, Batelle, Geneva, University of Warwick, Warwick, and Pitman Publishers, London, 1976; (*b*) A. E. R. Woodcock and T. A. Poston, in *Study of the Elementary Catastrophes*, Lecture Notes in Mathematics, Springer-Verlag, Berlin, 1974.
34 (*a*) J. Cioslowski, *J. Phys. Chem.*, 1990, **94**, 5496; (*b*) D. L. Cooper, *Nature* (*London*), 1990, **346**, 789; (*c*) G. I. Bersuker, C. Peng and J. E. Boggs, *J. Phys. Chem.*, 1993, **97**, 9323.
35 A. Savin, J. Jepsen, O. K. Andersen, H. Preuss and H. G. von Schnering, *Angew. Chem., Int. Ed. Engl.*, 1992, **31**, 187.
36 R. Abraham and J. E. Marsden, in *Foundations of Mechanics*, Addison-Wesley, New York, 2nd edn., 1987 and references cited therein.
37 R. Thom, in *Stabilité Structurelle et Morphogénèse*, Interéditions, Paris, 1972.
38 (*a*) S. G. Lias, J. E. Bartness, J. F. Liebman, J. L. Holmes, R. D. Levin and W. G. Mallard, *J. Phys. Chem. Ref. Data*, 1988, **117**, Suppl. 1; (*b*) C. E. Moore, in *Atomic Energy Levels*, National Bureau of Standards, Washington, DC, 1949, vol. 1; (*c*) C. E. Moore, in *Atomic Energy Levels*, National Bureau of Standards, Washington, DC, 1952, vol. 12.
39 R. Gilmore, in *Catastrophe Theory for Scientists and Engineers*, Dover Publications, New York, 1993.

Received in Montpellier, France, 4th March 1998;
Paper 8/01838C